Elasto-Plastic Transition in Epithelial Folding

Aki Teranishi[1], Misato Mori[2], Rihoko Ichiki[1], Satoshi Toda[2], Go Shioi[3], Satoru Okuda[2*]

[1] Division of Nano Life Science, Graduate School of Frontier Science Initiative, Kanazawa University, Kanazawa 920-1192, Japan

[2] Nano Life Science Institute, Kanazawa University, Kanazawa 920-1192, Japan

[3] RIKEN Center for Biosystems Dynamics Research, Kobe 650-0047, Japan

*** Corresponding author: satokuda@staff.kanazawa-u.ac.jp (S.O.)**

Abstract

During morphogenesis, epithelial sheets fold sequentially to make up three-dimensional organ structures. The resulting fold is irreversible, thereby allowing morphogenesis to proceed unidirectionally. However, how the irreversibility of folding is established remains unclear. We report a novel mechanical property of epithelia that is responsible for folding irreversibility. In e*x vivo* and *in vitro* cultures, epithelia exhibit an elastic response and restore their original shapes when folding is induced by short-term mechanical indentation. In contrast, long-term indentation induces a plastic response, resulting in irreversible deformation. Remarkably, the transition from an elastic to a plastic response occurs in a switch-like manner with a critical duration. This transition is established by the

accumulation of F-actin into a bracket-like structure across the fold, with the critical duration determined and tunable by the actin polymerization rate. Bracket formation and the resulting transition require two mechanosensing pathways: TRPC3/6-mediated calcium influx and ligand-independent epidermal growth factor receptor (EGFR) activation. While each pathway is independently triggered by deformation, calcium influx specifically occurs at the fold under EGFR activation. These results demonstrated that cells control epithelial folding irreversibility by detecting the temporal characteristics of deformation and adaptively switching between elastic and plastic responses. This finding, thus, resolves a long-standing question concerning the directionality of morphogenesis.

Main

Morphogenesis proceeds in one direction, with sequential epithelial folds transforming planar sheets into three-dimensional structures. Importantly, each fold is irreversible, and this irreversibility is essential for the formation of complex organ structures. Morphogenesis cannot proceed if the folds return to their original shapes; therefore, ensuring the irreversibility of epithelial folding is fundamental for achieving morphogenesis.

Various cellular behaviors that generate mechanical forces, including apical constriction, serve as key drivers of epithelial folding[1–5]. The balance between these forces and mechanical properties, such as elasticity and viscosity, determines the magnitude and rate of tissue deformations[6–10]. However, folding irreversibility cannot be explained by either driving forces or viscoelastic properties. Because the epithelium is constantly exposed to various deformations by the activities of its constituent cells and surrounding tissues[11–13], successful morphogenesis requires epithelia to retain necessary deformations while resisting unnecessary deformations.

We previously showed that the neuroepithelium has a bending plasticity that facilitates retinal invagination[14], suggesting that the bending plasticity of the epithelium can lead to irreversible morphological changes. The epithelium also displays bending elasticity that allows it to resist external forces[15–17]. Cells respond mechanosensitively to imposed deformations[18–21] and surrounding curvatures[22–24], indicating that cells may regulate their bending elasticity and plasticity — properties that confer opposing responses to external forces — to control the irreversibility of epithelial folding.

We developed a mechanical indentation assay for measuring the elastoplastic properties of the epithelium. We observed both elastic and plastic responses in several types of epithelia, including a mouse embryonic optic vesicle (OV), mouse embryonic stem cell (mESC)–derived OV organoid, and Madin-Darby canine kidney (MDCK) cell–derived cyst. Further experiments using the MDCK cell–derived cyst revealed an elastoplastic transition and its underlying molecular mechanisms, which likely serve to adaptively control the irreversibility of the epithelial folding response through the detection of imposed deformation.

Elastoplastic transition in folding

To measure epithelial bending plasticity, we developed an indentation assay, in which a glass pipette is used to indent the epithelium, forming a single fold. After holding the pipette in place for a defined time, the pipette is removed to relax the residual strain (**Fig. 1a,b** and **Extended Data Fig. 1a–e**). This assay enables the assessment of bending properties as a function of the hold duration (τ).

We first assessed the dependence of the bending property on τ. Mouse embryonic OV tissue exhibited an elastoplastic response dependent on τ: when τ = 20 sec, the tissue restored its original shape, whereas the tissue deformed irreversibly when τ = 30 min (**Fig. 1c** and **Supplementary Video 1**). A similar response was observed in mESC–derived OV organoids (**Fig. 1d** and **Supplementary Video 1**), indicating that this elastoplastic response is an intrinsic property of OVs, independent of surrounding tissues, such as the epidermis or the periocular mesenchyme. MDCK cell–derived cysts

displayed a similar elastoplastic response (**Fig. 1e** and **Supplementary Video 1**), suggesting that this response is not specific to mouse optic vesicles but is likely a general characteristic of many types of epithelia, including embryonic and cultured tissues. The plastic deformation that occurred after the 30-min indentation was maintained for several hours after unloading (**Extended Data Fig. 1b,f**).

In experiments using τ = 30 min, the tissue exhibited springback, in which a slight return to the original shape was observed after retraction, indicating a mixed elastic and plastic response. To quantify this mixed response, we introduced the degree of bending plasticity, ψ, based on the epithelial curvature measured at the fold caused by the indentation (see **Methods**). This criterion represents the contribution of plastic deformation to total deformation. Significant differences were observed between the elastic and plastic responses among embryonic OV tissues, mESC–derived OV organoids, and MDCK cell–derived cysts (**Fig. 1f**).

We performed further quantitative analyses using MDCK cell–derived cysts, which have consistent sizes and shapes and no surrounding tissues. The measurement revealed that ψ *is* dependent on τ, with an increase in τ associated with a monotonic increase in ψ, from elastic to plastic (**Fig. 1g**). Remarkably, the rate of increase in ψ is nonlinear, with a switch-like transition observed at a certain τ. By fitting a sigmoidal function, we identified the critical duration as τ_{ct} = 13 min. The original shape tended to be restored when τ was below τ_{ct}, whereas the tissue deformed irreversibly when τ was above τ_{ct}. These results show that the epithelium switches its bending response bistably between elastic and plastic depending on the temporal characteristics of the imposed deformation.

85

86 **Ligand-free mech-activated EGFR**

87 To understand how cells sense deformation, we measured ψ after the application of inhibitors. During
88 indentation, epidermal growth factor receptor (EGFR) becomes activated in a mechanosensitive
89 manner, and the inhibitors PD153035, LY294002, and ipatasertib, which inhibit EGFR,
90 phosphoinositide 3-kinase (PI3K), and Akt, respectively, all suppressed the elastoplastic transition (**Fig.**
91 **2a**), indicating that the EGFR–PI3K–Akt pathway regulates the transition.

92 The mitogen-activated protein kinase kinase (MEK) inhibitor PD325901 did not affect the
93 elastoplastic transition (**Fig. 2a** and **Extended Data Fig. 2a**), indicating that the MEK–ERK pathway
94 is not involved in the transition. However, the deformation activated extracellular signal-related kinase
95 (ERK), and this ERK activity was inhibited by EGFR inhibitor PD153035 (**Fig. 2d,f** and **Extended**
96 **Data Fig. 2a**), indicating that ERK activation occurred through EGFR. Therefore, to monitor the
97 EGFR activation in the transition, we utilized a Förster resonance energy transfer (FRET) sensor for
98 ERK activation (**Fig. 2b**, **Extended Data Fig. 2a** and **Supplementary Video 2**). The FRET ratio
99 increased rapidly within the first 5 min of indentation, particularly near the fold (**Fig. 2b,c**), followed
100 by a gradual decrease (**Fig. 2d**).

101 To clarify what triggers EGFR activation, we assessed cysts derived from MDCK cells engineered
102 to knock out all endogenous EGFR ligands: epidermal growth factor (EGF), transforming growth
103 factor alpha (TGFα), heparin-binding EGF-like growth factor (HBEGF), and epiregulin (EREG)[25].

104 These cysts displayed an increased FRET ratio and elastoplastic transition in response to deformation
105 (**Fig. 2e,f**), and similar results were obtained in cysts derived from MDCK cells engineered to knock
106 out only EGF and those engineered to knock out disintegrin and metalloprotease 17 (ADAM17), in
107 which TGFα, HBEGF, and EREG are inactivated (**Fig. 2e,f** and **Extended Data Fig. 2a-e**). These
108 results show that deformation triggers EGFR activity in a ligand-independent manner.

109 Our findings indicate that the elastoplastic transition involves the mechanosensitive and ligand-
110 independent activation of the EGFR–PI3K–Akt pathway, which is consistent with previous reports that
111 EGFR is activated without a ligand[26–28] and in a mechanosensitive manner[29–31].

112

113 **Mech-induced calcium transient at fold**

114 Our inhibitor assays revealed that mechanosensitive calcium channels are required for elastoplastic
115 transition. The transition was suppressed by the inhibition of mechanosensitive cation channels,
116 including transient receptor potential canonical (TRPC)1/6, using Grammostola
117 mechanotoxin 4 (GsMTx4)[32,33], and by the chelation of intracellular calcium, using BAPTA-AM (**Fig.**
118 **3a** and **Extended Data Fig. 3**). Specifically, the transition was suppressed by the inhibition of TRPC6
119 with SAR-7334; however, it still occurred even under the inhibition of TRPC1 with Pico145 (**Fig. 3a**
120 and **Extended Data Fig. 3**), indicating that TRPC6-mediated calcium influx is necessary for the
121 transition. Moreover, TRPC3 and TRPC6 form a heteromeric complex on the apical side[34], and

122 inhibition of TRPC3 with Pyr3 suppressed the transition (**Fig. 3a**), suggesting that cells detect
123 deformation via TRPC3/6-mediated calcium influx on the apical side.

124 We performed live intracellular calcium imaging to observe the spatial pattern of calcium influx
125 using cysts derived from a cell line stably expressing the calcium indicator GCaMP6s. We found that
126 indentation induced typical calcium transients (**Fig. 3b,c** and **Supplementary Video 3**) that were
127 maintained throughout the indentation duration. These transients were specifically localized at the
128 apical side of the fold (**Fig. 3d,e,f**) in a region measuring approximately 20.7 μm long along the
129 contour and approximately 5.0 μm thick along the apicobasal axis (**Extended Data Fig. 3c–e**). These
130 transients were suppressed by GsMTx4 and BAPTA-AM (**Fig. 3g** and **Extended Data Fig. 3a,b**),
131 which corresponds to the suppression of the transition by these inhibitors (**Fig. 3a**). These findings
132 show that cells detect folding on the apical side via mechanosensitive calcium influx.

133 We also assessed the interaction between EGFR activation and calcium influx. To clarify whether
134 EGFR activation affects calcium signaling, we performed live calcium imaging of cysts derived from
135 GCaMP6s-expressing cells treated with the EGFR inhibitor PD153035, which revealed that PD153035
136 suppressed chronic calcium transients (**Fig. 3g** and **Extended Data Fig. 3**). By contrast, we observed
137 increased FRET in response to indentation in the presence of the mechanosensitive channel inhibitor
138 GsMTx4 (**Fig. 3h** and **Extended Data Fig. 2**). These results indicate that the elastoplastic transition
139 requires both mechanosensitive pathways: EGFR activation and calcium influx. While both of them

140 are independently triggered by deformation, calcium influx is triggered under EGFR activation.
141 Through the calcium pathway, cells detect apical deformation.
142
143 **Actin bracket establishes the transition**
144 To elucidate the mechanism that establishes the transition, we performed live imaging of F-actin using
145 cysts derived from an MDCK cell line, stably expressing mCherry-fused Lifeact. During indentation,
146 F-actin gradually accumulated locally at the apical side of the fold (**Fig. 4a, Extended Data Fig. 4a**,
147 **Supplementary Video 4**). Three-dimensional imaging revealed F-actin accumulation not only on the
148 apical side but also along the lateral boundaries between cells (**Extended Data Fig. 4b** and
149 **Supplementary Video 5**). F-actin accumulated to form a bracket-like structure along the apical side
150 of the epithelium, which we term the 'actin bracket,' approximately 9.6 μm long and 2.0 μm thick (**Fig.**
151 **4b**,**c, Extended Data Fig. 4c-e**), corresponding to the region with frequent calcium transients
152 (**Extended Data Fig. 3c-e**).
153 F-actin accumulation occurred most rapidly at the point of highest curvature, showing a linear
154 increase for the first 10 min and then plateauing (**Fig. 4d**). This time duration is shorter than the critical
155 duration for the elastoplastic transition (**Fig. 1g**). The region of accumulation gradually expanded from
156 this point, taking approximately 16 min to fully form the actin bracket and cover the fold (**Fig. 4d**).
157 This time duration corresponds to the critical duration of the transition (**Fig. 1g**), indicating that the
158 formation of the actin bracket is essential for the transition.

159 To clarify the role of F-actin accumulation in the elastoplastic transition, we measured ψ following
160 the inhibition of F-actin polymerization with cytochalasin D, latrunculin A, or CK-666 (**Fig. 4e** and
161 **Extended Data Fig. 5**). These inhibitors not only suppressed F-actin accumulation but also inhibited
162 the transition, indicating the critical role of F-actin polymerization. In addition, inhibiting the EGFR-
163 PI3K–Akt and calcium pathways, which are known regulators of F-actin dynamics[35–39], also halted
164 both F-actin accumulation and the transition (**Fig. 2a,3a,4e** and **Extended Data Fig. 5**). By contrast,
165 inhibiting MEK or TRPC1 had no effect on F-actin accumulation, corresponding to the lack of effect
166 on the transition. These results indicate that F-actin accumulation, regulated downstream of EGFR–
167 PI3K–Akt and calcium pathways, is essential for the elastoplastic transition.

168 Interestingly, enhancing actin polymerization with jasplakinolide resulted in a plastic response as
169 rapidly as 5 min after indentation (**Fig. 4e** and **Extended Data Fig. 5**). Even in the presence of
170 jasplakinolide, short-term indentations induced elastic responses, but the critical duration required for
171 the elastoplastic transition (τ_{ct} = 2.8 min) was significantly shorter than under untreated conditions (**Fig.**
172 **4f**). This result indicates that the actin polymerization rate determines the critical duration required for
173 elastoplastic transition.

174 These results show that F-actin accumulates across the fold, forming a bracket-like structure that
175 establishes elastoplastic transition, and that the critical duration can be tuned by adjusting the actin
176 polymerization rate.

177

Discussion

In this study, we elucidated the mechanism underlying elastoplastic transition during epithelial folding, which occurs as an all-or-nothing response that is dependent on the temporal characteristics of the imposed deformation. The transition is established by the accumulation of F-actin in response to mechanosensing pathway activation (**Extended Data Fig. 6**).

The concept of elastoplastic transition is well-known in the field of solid materials engineering. However, its mechanics in epithelial folding have not been previously reported, to our knowledge. Metals and resins typically exhibit strain-dependent elastoplastic transitions, with plastic deformation resulting from large deformations[40]. By contrast, elastoplastic transitions for fabrics and other materials are often time-dependent transitions, with the transition duration dependent on the material and environment. Transitions in these materials are generally caused by passive mechanisms, such as atomic displacement in metals, crystal exfoliation in resins, and fiber displacement in fabrics (**Extended Data Fig. 7a**). The tunable critical duration in epithelial folding, as regulated by living cells, represents a sharp contrast with the transition mechanics associated with other materials.

The elastoplastic transition of the epithelium is analogous to tissue fluidization[41–44], as both of these processes are able to induce irreversible deformation (**Extended Data Fig. 7b**). However, fluidization requires tissue to phase transition from a solid to a liquid, whereas tissue remains in the solid phase during the elastoplastic transition. Kinematically, fluidization is caused by a global rearrangement of cells at the tissue scale, whereas the elastoplastic transition is caused by a change in

local cell behavior and does not require global rearrangement. In the elastoplastic transition, local cell behavior alone can cause tissue-scale deformation, generating an irreversible fold structure.

The cells that drive apical constriction in epithelial folding may also undergo elastoplastic transition, responding to their own deformation (**Extended Data Fig. 7c**). This idea is supported by observations that elastoplastic transition and apical constriction share several key components, including actomyosin activity[1–3,14,45–48], calcium signaling[14,46], and EGFR activation[47–49]. Apical constriction occurs collectively for all cells within a specific region and period; however, individual cells are constantly generating relatively short-term forces through behaviors such as division, apoptosis, and contraction, which can introduce noise[44,50]. Elastoplastic transition may play a key role in stabilizing appropriate invaginations, filtering out the noise from short-term individual cell forces, and enabling collective cellular behaviors.

In conclusion, we demonstrated that cells actively control the irreversibility of epithelial folding through the elastoplastic transition. This observation requires the reconsideration of long-standing mechanistic concepts in development, indicating that epithelial morphogenesis proceeds not only by regulating active force generation but also by regulating deformation irreversibility to define the resulting morphology.

Acknowledgments

We thank all the members of Okuda's laboratory for discussions; S. Hayashi, Y. C. Wang, and F. Motegi for critical reading; M. Matsuda and K. Okamoto for valuable comments; K. Yoshida for help with experiments; and A. Matsuoka for help with image analysis. This work was supported by the WISE Program for Nano-Precision Medicine, Science, and Technology of Kanazawa University, Ministry of Education, Culture, Sports, Science and Technology (MEXT; to AT); the Japan Science and Technology Agency (JST), CREST [Grant No. JPMJCR1921]; the Japan Agency for Medical Research and Development [AMED; Grant No. 21bm0704065h0003]; the Japan Society for the Promotion of Science (JSPS), KAKENHI [Grants No. 21H01209, 21KK0134, 22K18749, and 22H05170]; and the World Premier International Research Center Initiative, MEXT, Japan (to SO).

Author contributions

A.T.: data curation, formal analysis, investigation, methodology, resources, software, validation, visualization, and writing (original draft and revised draft). M.M.: formal analysis and investigation. R.I.: investigation and validation. S.T.: resources and validation. G.S.: resources and validation. S.O.: conceptualization, data curation, formal analysis, funding acquisition, methodology, project administration, resources, software, supervision, visualization, and writing (original draft and revised draft).

Competing interests

The authors declare no competing interests.

Correspondence and requests for materials should be addressed to Satoru Okuda.

Main References

1. Martin, A. C. & Goldstein, B. Apical constriction: themes and variations on a cellular mechanism driving morphogenesis. *Development* **141**, 1987–1998 (2014).
2. Sawyer, J. M. *et al.* Apical constriction: a cell shape change that can drive morphogenesis. *Dev Biol* **341**, 5–19 (2010).
3. Martin, A. C., Kaschube, M. & Wieschaus, E. F. Pulsed contractions of an actin–myosin network drive apical constriction. *Nature* **457**, 495–499 (2009).
4. Kondo, T. & Hayashi, S. Mitotic cell rounding accelerates epithelial invagination. *Nature* **494**, 125–129 (2013).
5. Takeichi, M. Dynamic contacts: rearranging adherens junctions to drive epithelial remodelling. *Nat Rev Mol Cell Biol* **15**, 397–410 (2014).
6. von Dassow, M. & Davidson, L. A. Variation and robustness of the mechanics of gastrulation: the role of tissue mechanical properties during morphogenesis. *Birth Defects Res C Embryo Today* **81**, 253–269 (2007).
7. Davidson, L. A. *et al.* Emergent morphogenesis: elastic mechanics of a self-deforming tissue. *J Biomech* **43**, 63–70 (2010).
8. Khalilgharibi, N. *et al.* Stress relaxation in epithelial monolayers is controlled by the actomyosin cortex. *Nat Phys* **15**, 839–847 (2019).

9. Mongera, A. *et al.* Mechanics of the cellular microenvironment as probed by cells in vivo during zebrafish presomitic mesoderm differentiation. *Nat Mater* **22**, 135–143 (2023).

10. He, B., Doubrovinski, K., Polyakov, O. & Wieschaus, E. Apical constriction drives tissue-scale hydrodynamic flow to mediate cell elongation. *Nature* **508**, 392–396 (2014).

11. Mao, Y. & Baum, B. Tug of war—the influence of opposing physical forces on epithelial cell morphology. *Dev Biol* **401**, 92–102 (2015).

12. Davidson, L. A. Epithelial machines that shape the embryo. *Trends Cell Biol* **22**, 82–87 (2012).

13. Matamoro-Vidal, A. & Levayer, R. Multiple influences of mechanical forces on cell competition. *Current Biology* **29**, R762–R774 (2019).

14. Okuda, S. *et al.* Strain-triggered mechanical feedback in self-organizing optic-cup morphogenesis. *Sci Adv* **4**, eaau1354 (2018).

15. Davidson, L. A. Embryo mechanics: balancing force production with elastic resistance during morphogenesis. *Curr Top Dev Biol* **95**, 215–241 (2011).

16. Harris, A. R. *et al.* Characterizing the mechanics of cultured cell monolayers. *Proceedings of the National Academy of Sciences* **109**, 16449–16454 (2012).

17. Latorre, E. *et al.* Active superelasticity in three-dimensional epithelia of controlled shape. *Nature* **563**, 203–208 (2018).

18. Discher, D. E., Janmey, P. & Wang, Y. Tissue cells feel and respond to the stiffness of their substrate. *Science (1979)* **310**, 1139–1143 (2005).

19. Vogel, V. & Sheetz, M. Local force and geometry sensing regulate cell functions. *Nat Rev Mol Cell Biol* **7**, 265–275 (2006).

20. Mao, Y. *et al.* Differential proliferation rates generate patterns of mechanical tension that orient tissue growth. *EMBO J* **32**, 2790–2803 (2013).

21. Coste, B. *et al.* Piezo proteins are pore-forming subunits of mechanically activated channels. *Nature* **483**, 176–181 (2012).

22. Baptista, D., Teixeira, L., van Blitterswijk, C., Giselbrecht, S. & Truckenmüller, R. Overlooked? Underestimated? Effects of substrate curvature on cell behavior. *Trends Biotechnol* **37**, 838–854 (2019).

23. Luciano, M. *et al.* Cell monolayers sense curvature by exploiting active mechanics and nuclear mechanoadaptation. *Nat Phys* **17**, 1382–1390 (2021).

24. Tang, W. *et al.* Collective curvature sensing and fluidity in three-dimensional multicellular systems. *Nat Phys* **18**, 1371–1378 (2022).

25. Lin, S. *et al.* Redundant roles of EGFR ligands in the ERK activation waves during collective cell migration. *Life Sci Alliance* **5**, (2022).

26. Guo, G. *et al.* Ligand-independent EGFR signaling. *Cancer Res* **75**, 3436–3441 (2015).

27. Lambert, S., Vind-Kezunovic, D., Karvinen, S. & Gniadecki, R. Ligand-independent activation of the EGFR by lipid raft disruption. *Journal of Investigative Dermatology* **126**, 954–962 (2006).

292 28. Moro, L. *et al.* Integrin-induced epidermal growth factor (EGF) receptor activation requires c-
293 Src and p130Cas and leads to phosphorylation of specific EGF receptor tyrosines. *Journal of*
294 *Biological Chemistry* **277**, 9405–9414 (2002).
295 29. Rao, T. C. *et al.* EGFR activation attenuates the mechanical threshold for integrin tension and
296 focal adhesion formation. *J Cell Sci* **133**, jcs238840 (2020).
297 30. Saxena, M. *et al.* EGFR and HER2 activate rigidity sensing only on rigid matrices. *Nat Mater*
298 **16**, 775–781 (2017).
299 31. Umesh, V., Rape, A. D., Ulrich, T. A. & Kumar, S. Microenvironmental stiffness enhances
300 glioma cell proliferation by stimulating epidermal growth factor receptor signaling. *PLoS One*
301 **9**, e101771 (2014).
302 32. Bae, C., Sachs, F. & Gottlieb, P. A. The mechanosensitive ion channel Piezo1 is inhibited by
303 the peptide GsMTx4. *Biochemistry* **50**, 6295–6300 (2011).
304 33. Gailly, P. TRP channels in normal and dystrophic skeletal muscle. *Curr Opin Pharmacol* **12**,
305 326–334 (2012).
306 34. Bandyopadhyay, B. C. *et al.* Apical localization of a functional TRPC3/TRPC6-Ca2+-signaling
307 complex in polarized epithelial cells: role in apical Ca2+ influx. *Journal of Biological*
308 *Chemistry* **280**, 12908–12916 (2005).
309 35. Liang, C. *et al.* Towards an integrative understanding of cancer mechanobiology: calcium, YAP,
310 and microRNA under biophysical forces. *Soft Matter* **18**, 1112–1148 (2022).

311 36. Sanderson, M. J., Charles, A. C. & Dirksen, E. R. Mechanical stimulation and intercellular
312 communication increases intracellular Ca2+ in epithelial cells. *Cell Regul* **1**, 585–596 (1990).
313 37. Liu, J. *et al.* PI3K/Akt-dependent phosphorylation of GSK3β and activation of RhoA regulate
314 Wnt5a-induced gastric cancer cell migration. *Cell Signal* **25**, 447–456 (2013).
315 38. Deng, S. *et al.* PI3K/AKT Signaling Tips the Balance of Cytoskeletal Forces for Cancer
316 Progression. *Cancers (Basel)* **14**, 1652 (2022).
317 39. Qian, Y. *et al.* PI3K induced actin filament remodeling through Akt and p70S6K1: implication
318 of essential role in cell migration. *American Journal of Physiology-Cell Physiology* **286**, C153–
319 C163 (2004).
320 40. Courtney, T. H. Embrittlement. *Mechanical Behavior of Materials, Second ed., McGraw-Hill*
321 *International Editions, Singapore* 630–685 (2000).
322 41. Krajnc, M., Dasgupta, S., Ziherl, P. & Prost, J. Fluidization of epithelial sheets by active cell
323 rearrangements. *Phys Rev E* **98**, 22409 (2018).
324 42. Petridou, N. I., Grigolon, S., Salbreux, G., Hannezo, E. & Heisenberg, C.-P. Fluidization-
325 mediated tissue spreading by mitotic cell rounding and non-canonical Wnt signalling. *Nat Cell*
326 *Biol* **21**, 169–178 (2019).
327 43. Tetley, R. J. *et al.* Tissue fluidity promotes epithelial wound healing. *Nat Phys* **15**, 1195–1203
328 (2019).

329 44. Ranft, J. *et al.* Fluidization of tissues by cell division and apoptosis. *Proceedings of the National*
330 *Academy of Sciences* **107**, 20863–20868 (2010).
331 45. Lecuit, T. & Lenne, P.-F. Cell surface mechanics and the control of cell shape, tissue patterns
332 and morphogenesis. *Nat Rev Mol Cell Biol* **8**, 633–644 (2007).
333 46. Suzuki, M. *et al.* Distinct intracellular Ca2+ dynamics regulate apical constriction and
334 differentially contribute to neural tube closure. *Development* **144**, 1307–1316 (2017).
335 47. Ogura, Y., Wen, F.-L., Sami, M. M., Shibata, T. & Hayashi, S. A switch-like activation relay of
336 EGFR-ERK signaling regulates a wave of cellular contractility for epithelial invagination. *Dev*
337 *Cell* **46**, 162–172 (2018).
338 48. Hirashima, T. & Matsuda, M. ERK-mediated Curvature Feedback Regulates Branching
339 Morphogenesis in Lung Epithelial Tissue. *BioRxiv* (2022).
340 49. Brodu, V. & Casanova, J. The RhoGAP crossveinless-c links trachealess and EGFR signaling
341 to cell shape remodeling in Drosophila tracheal invagination. *Genes Dev* **20**, 1817–1828 (2006).
342 50. Levayer, R. & Lecuit, T. Oscillation and Polarity of E-Cadherin Asymmetries Control
343 Actomyosin Flow Patterns during Morphogenesis. *Dev Cell* **26**, 162–175 (2013).
344

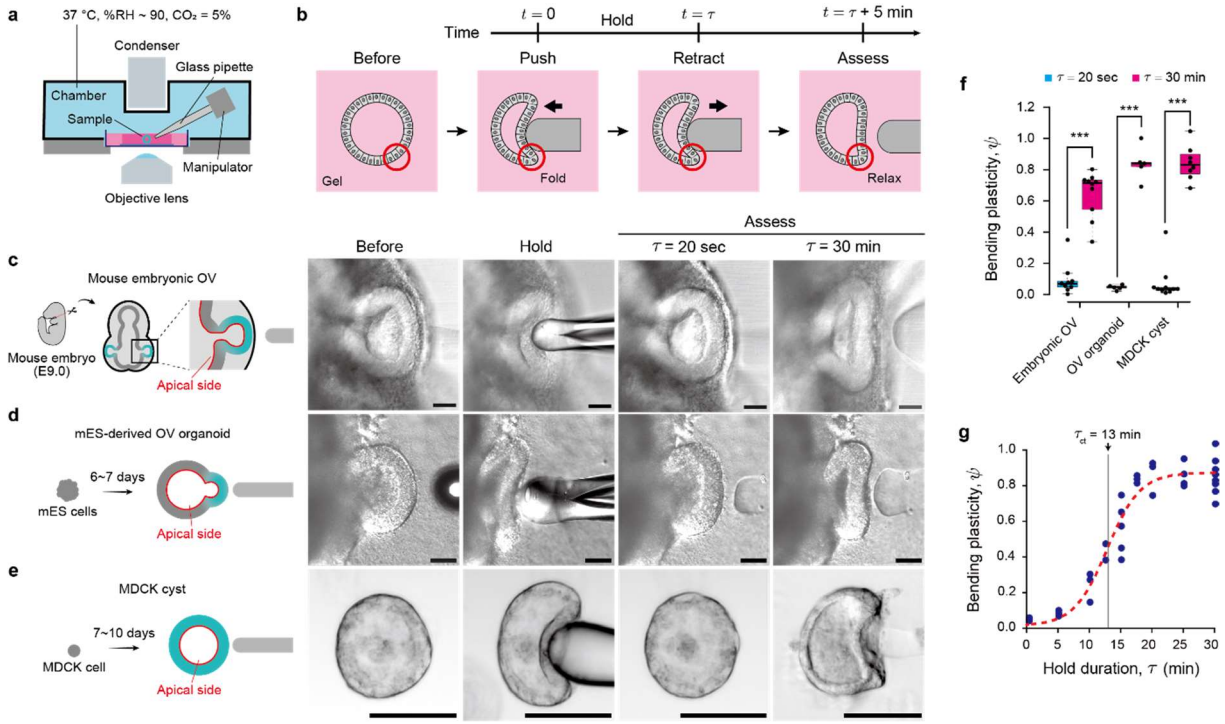

Fig. 1 Epithelial folding shows a switch-like transition from elastic to plastic responses. a, Mechanical indentation device with a custom culture chamber on a confocal microscope. An electric piezo manipulator with a glass pipette is placed inside. **b**, Schematic for the flow of the indentation assay. Bending plasticity, ψ, was introduced, and its dependence on the hold duration, τ, was explored. **c–e**, Schematics and images of the epithelium before, during, and after indentation for (**c**) mouse embryonic optic vesicles (OVs) at E9.0, (**d**) an OV organoid derived from mouse embryonic stem cells (mESCs) at Day 6 or 7, and (**e**) a cyst derived from Madin-Darby canine kidney (MDCK) cells. Scale bar, 50 µm. **f**, Bending plasticity, ψ, of three types of epithelia ($N \geq 7$). Box plots in (**f**): center: median; bounds, 25th and 75th percentiles; whiskers, min and max; ***$P < 0.001$ (Welch's t-test). **g**, Bending plasticity, ψ, of MDCK cell–derived cysts as a function of τ. Red dotted line shows a sigmoid function fitted by the least squares method, in which critical duration, τ_{ct}, is 13 min.

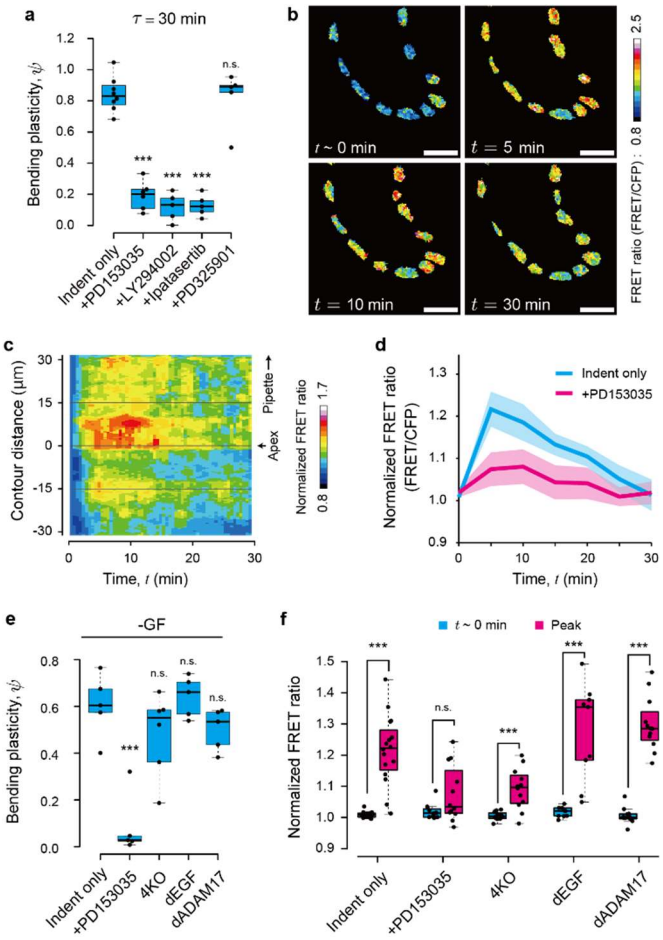

Fig. 2 Ligand-independent, mechanically activated EGFR and PI3K–Akt pathway induces elastoplastic transition. a, Bending plasticity, ψ, for indentation only and indentation in the presence of inhibitors for EGFR or downstream molecules, at τ = 30 min (N ≥ 5). **b**, ERK-FRET images for indentation only immediately after initiation, at the time of peak ratio, and 30 min after indentation. Scale bars, 15 μm. **c**, Kymograph of ERK-FRET ratio along the epithelium contour over time under conditions of indentation only. FRET ratio at each pixel is normalized to its value immediately after indentation and averaged across samples (N = 5). The pipette is at a positive distance from the apex with the highest curvature. **d**, Time variations of ERK-FRET ratios around the apex during indentation for indentation only and indentation in the presence of EGFR inhibition (N = 8). Data represent the

mean ± s.e. **e**, Bending plasticity, ψ, in cysts featuring the knockout of EGFR agonists, including all four factors (4KO), EGF (dEGF), and a factor upstream of the other three agonists (dADAM17), for τ = 30 min (N ≥ 5). **f**, ERK-FRET ratios of cysts featuring the knockout of EGFR agonists at t = 0 min and the time of peak ratio (N ≥ 5). Box plots in **a**, **e**, and **f**: center, median; bounds, 25th and 75th percentiles; whiskers, min and max; ***P < 0.001 (Welch's t-test). ADAM17, a disintegrin and metalloproteinase 17; EGF, epidermal growth factor; EGFR, epidermal growth factor receptor; ERK, extracellular signal-related kinase; FRET, Förster resonance energy transfer; PI3K, phosphoinositide 3-kinase.

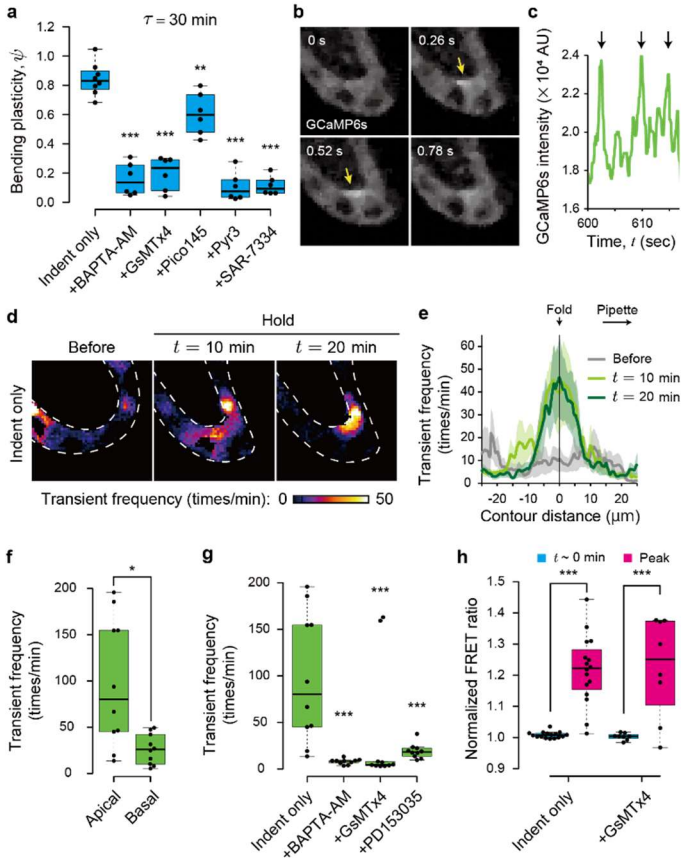

Fig. 3 TRPC3/6-mediated calcium transient induces elastoplastic transition by detecting apical deformation. a, Bending plasticity, ψ, under conditions of mechanosensitive channel inhibition or intracellular calcium chelation for $\tau = 30$ min ($N \geq 6$). **b**, Time-lapse images of GCaMP6s 10 min after indentation initiation. Calcium transients occurred in the apical region (arrows). **c**, Time variations of calcium concentrations around the apex 10 min after indentation initiation. **d** and **e**, Spatial distributions of calcium transient frequency: before, 10 min, and 20 min after indentation initiation. Map view (**d**) and distribution along the epithelium contour averaged across samples (**e**). Dotted lines indicate epithelium contours. Data represent the mean ± s.e. (N = 5). **f**, Calcium transient frequency at apical and basal regions (N = 5). **g**, Calcium transient frequency around the apex under conditions of mechanosensitive channel inhibition, intracellular calcium chelation, or EGFR inhibition (N = 5). **h**,

ERK-FRET ratios under conditions of mechanosensitive channel inhibition at $t = 0$ and the time of peak ratio (N = 7). Box plots in **a** and **e**–**h**): center, median; bounds, 25th and 75th percentiles; whiskers, min and max; *P < 0.05, **P < 0.01, ***P < 0.001 (Welch's t-test). EGFR, epidermal growth factor receptor; ERK, extracellular signal-related kinase; FRET, Förster resonance energy transfer; TRPC, transient receptor potential canonical**.**

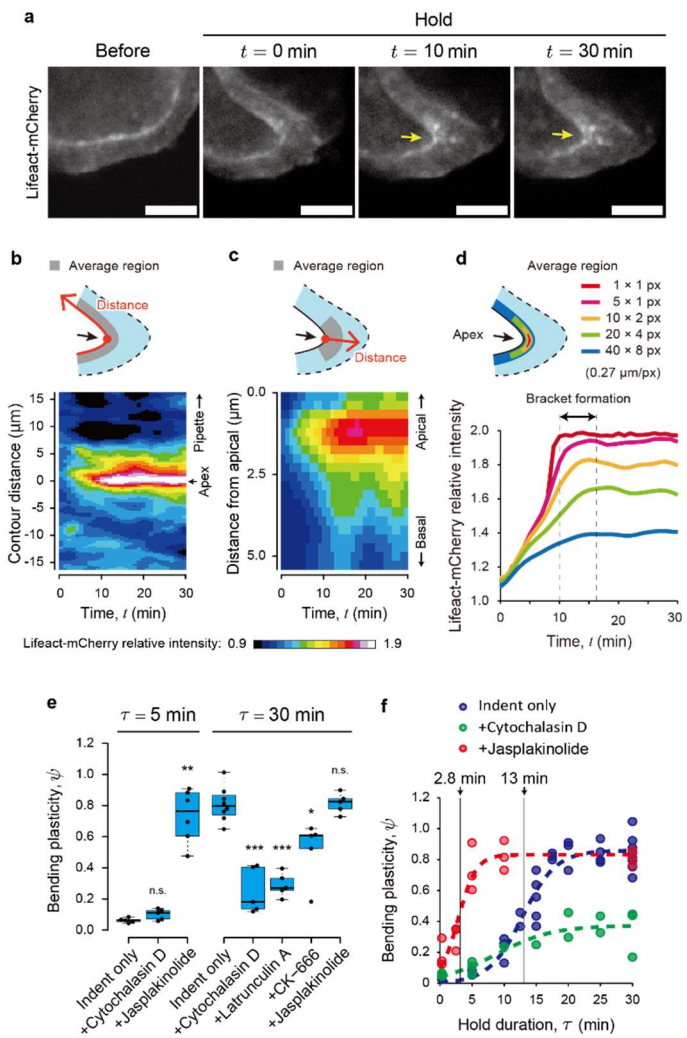

Fig. 4 Local F-actin accumulation forms a bracket-like structure that is essential for elastoplastic transition. a, Time-lapse images of Lifeact-mCherry before indentation and at t = 0 min, t = 10 min, and t = 30 min. F-actin accumulated at fold (arrows). Scale bars, 15 μm. **b** and **c**, Kymographs of Lifeact-mCherry intensity along the epithelium contour (**b**) and apicobasal axis (**c**) over time. Intensity at each pixel was normalized to the initial intensity and averaged across samples (N = 5). **d**, Time variation of the maximum and average Lifeact-mCherry intensity around fold (N = 5). **e**, Bending plasticity, ψ, under conditions of F-actin dynamics inhibition for τ = 5 min and τ = 30 min (N ≥ 5). **f**, Bending plasticity, ψ, as a function of duration time, τ, under conditions of actin polymerization

400 inhibition or enhancement. Dotted lines show fitted sigmoid functions. Box plots in **f**: center, median;

401 bounds, 25th and 75th percentiles; whiskers, min and max; *P < 0.05, **P < 0.01, ***P < 0.001

402 (Welch's t-test). EGFR, epidermal growth factor receptor.